


ARTICLE

<https://doi.org/10.1038/s42004-019-0169-5>

OPEN

A self-powered electrolytic process for glucose to hydrogen conversion

Yongfeng Li^{1,2,3} , Wei Liu^{1,3}, Zhe Zhang¹, Xu Du¹, Lin Yu² & Yulin Deng¹

Glucose is a promising feedstock for hydrogen production but the existing microbial electrolysis process suffers from low efficiency. Here we show a process for hydrogen production using an integrated device consisting of a liquid-catalyst fuel cell (LCFC) stack and a polymer exchange membrane electrolytic cell (PEMEC). Glucose that cannot be directly used in traditional fuel cell was used as both the fuel to power the LCFC and the hydrogen sources. Different from simple combination of two independent units, the LCFC and PEMEC in our device are dependant one on another by using a SHAREDCELL, and all electrolytes in both fuel cell and electrolyzer are self-regenerated without using external electricity. As a result, feed stock of glucose was converted to pure hydrogen in cathode, and carbon dioxide in anode. The net reaction of the process is that glucose decomposes to hydrogen and carbon dioxide under thermal heating at -85 °C.

¹School of Chemical & Biomolecular Engineering and RBI at Georgia Tech, Georgia Institute of Technology, Atlanta, GA 30332-0620, USA. ²School of Chemical Engineering and Light Industry, Guangdong University of Technology, Guangzhou 510006 Guangdong, PR China. ³These authors contributed equally: Yongfeng Li, Wei Liu. Correspondence and requests for materials should be addressed to Y.D. (email: yulin.deng@rbi.gatech.edu)

Hydrogen as a clean, renewable and sustainable energy carrier has been considered as the most promising source of energy that can be used in both internal combustion engines and fuel cells with no toxic gas formation^{1,2}. Currently, over 95% of hydrogen production comes from the fossil fuels such as natural gas steam reforming, coal or biomass gasification and heavy oil partial oxidation processes^{3,4}. In the pursuit of a secure and clean future for hydrogen economy, environmentally benign hydrogen production from abundant, clean and renewable sources must be developed. Although steam reforming is an energy efficient and low cost technology, the steam reforming plant is usually a huge plant, so considerable raw materials are needed to maintain its daily operation. This is a critical problem if biomass is used as the hydrogen source because of the high cost in biomass collection and transportation. Therefore, a novel technology that can be used to build an economic and profitable medium or small unit for hydrogen production is of great interest to the engineers and scientists.

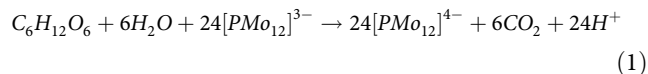
Biomass is considered an ideal CO₂ neutral, abundant and renewable organic substitute to fossil fuel^{5,6}. Nowadays, fast/flash biomass pyrolysis and steam gasification at high temperature of 600–1000 °C can offer fast and high stoichiometric yield of hydrogen, providing a promising mean of large-scale hydrogen generation from biomass^{7–10}, but the techniques suffer from the problems of high operating temperature and low-quality/impurity of produced H₂-rich gases^{7,9,11}. Biomass collection and transportation to large steam reforming plants also restricts their operation. On the other hand, biomass dark fermentation can produce H₂-rich gases at ambient temperature^{12,13}. However, the hydrogen production rate is very low due to the low degradation degree of biomass fermentation, and the impurity is high because of the presence of other gas products^{14–16}. For example, over 80% of the end-products are acetic and butyric acids with glucose as model substrate in dark fermentation¹². Recently, a new biological method, microbial electrolysis cell (MEC), can convert simple acetate and glucose into pure H₂ gas using current generated by exoelectrogenic microbes^{17–21}. However, an external voltage of 0.2–0.8 V must be applied to the electrolysis cell to overcome the thermodynamic barrier of electrolysis reaction¹⁷, and the hydrogen production rate is still low (just 2.39 m³ H₂/m³/d based on MEC volume), which should be ascribed to the low reaction rate between exoelectrogenic microbes and biomass feedstock²².

Herein, we report an integrated device combining fuel cell stack and electrolysis cell, in which glucose-based fuel cell stack provides current and voltage to electrolysis cell for hydrogen evolution. Polyoxometalate (POM) is used to replace exoelectrogenic microbe as the catalyst, which can rapidly oxidize glucose and be completely self-regenerated during the process. Our system uses a “SHAREDCELL” between fuel cell cathode and electrolyzer anode. With this unique design, fuel cell cathode electrolyte (Fe³⁺) is self-regenerated by the anode of electrolyzer and simultaneously by oxygen in air. As a result, glucose in electrolysis cell can be effectively converted to pure H₂ gas at a low temperature of 85 °C by self-powered electric energy. Moreover, a high hydrogen production rate of 0.0432 mL/cm²/min (or 62.2 m³ H₂/m³/d) based on the electrolysis cell volume can be achieved in the integrated device.

Results

The integrated device. This integrated device is schematically shown in Fig. 1 and the photographs of experiment setup are shown in Supplementary Fig. 1. The device includes four key units: REACTOR, liquid-catalyst fuel cells (LCFCs), polymer exchange membrane electrolytic cell (PEMEC), and SHAREDCELL.

The feedstock of glucose is mixed with POM catalyst in the REACTOR. A simple Keggin-structure POM catalyst, phosphomolybdic acid solution (noted as PMo₁₂) was used in this study. In the REACTOR unit, glucose is oxidized and degraded to CO₂ by oxidation of PMo₁₂ under thermal heating



As a result, one [PMo₁₂]³⁻, noted as [POM]³⁻, captures one electron and is reduced to [PMo₁₂]⁴⁻ (noted as [POM]⁴⁻), and simultaneously one proton ion is released from glucose. It should be noted that the above reaction is based on the assumption that one PMo₁₂ will receive only one electron, (i.g. the reduction degree is 1). Actually, one POM can receive more than one electron because their 12 Mo^{VI} ions in one POM molecules. The electrons that one mole POM received during the reaction is called reduction degree^{23,24}. In our experimental condition, the reduction degree of POM is in the range of 2–3.5 depending on the reaction time and temperature, concentration etc.

The LCFC is similar to the devices reported in our previous studies^{23–25}, which was constructed using a Nafion 115 membrane sandwiched between two 3D graphite electrodes with no metal loading. The reduced [POM]⁴⁻ from the REACTOR functions as anode electrolyte which supplies electrons to the carbon anode in the LCFC, and Fe³⁺ functions as cathode oxidation agent, as shown in Fig. 1. It is noted that the [POM]³⁻/[POM]⁴⁻ redox pair at a concentration of ~0.5 M has an electrochemical potential ranges from +0.38 to +0.45 V relative to the standard hydrogen electrode (SHE)²⁶, and Fe³⁺/Fe²⁺ redox pair has a standard electrochemical potential +0.77 V. Clearly, Fe³⁺ can oxidize reduced [POM]⁴⁻ to [POM]³⁻, and itself will be reduced to Fe²⁺. Therefore, a fuel cell consist of two redox pairs of [POM]³⁻/[POM]⁴⁻ and Fe³⁺/Fe²⁺ can be fabricated, as shown in Fig. 1. Practically, [POM]⁴⁻ at anode side gives the electrons through external circuit to cathode side, and simultaneously releases protons as charge-balancing ions. The protons are then penetrates through Nafion membrane to the cathode cell where Fe³⁺ captures the electrons to form Fe²⁺. Meanwhile, the feedstock of glucose in the REACTOR continuously reacts with the regenerated [POM]³⁻ to keep a stable reaction state. (The detail electro-chemical reactions in the entire device will be discussed later).

The PEMEC is sandwiched between a simple carbon anode without coating any catalyst and a carbon cathode coated with Pt black catalyst (ca. 2 mg cm⁻²) for hydrogen evolution. There is a SHAREDCELL between LCFC and PEMEC in which Fe³⁺/Fe²⁺ pair is used as cathode electrolyte for LCFC and anode electrolyte for PEMEC. As discussed above, Fe³⁺ ions are oxidation agent in the LCFC (on cathode), but Fe²⁺ ions in the SHAREDCELL functions as a reducing agent in PEMEC (on anode) which release electrons to external circuit and are oxidized back to Fe³⁺ ions. The electrons and protons from anode of the LCFC are transferred to the cathode of PEMEC in which they combine to form hydrogen gas.

The SHAREDCELL refers to the SHAREDCELL between LCFCs and PEMEC, in which the Fe³⁺/Fe²⁺ electrolyte solution is shared by the cathode of LCFCs and the anode of PEMEC. As discussed above, the open cell voltage of one fuel cell is ~0.35 V, which is not high enough to split water in an acid PEMEC solution. Therefore, multi-fuel cells are assembled together in series to form a cell stack.

Using a three fuel cell stack as an example, the actual electronic circuit is shown in Fig. 1b. When one electron is given from the LCFCs stack, there would generate one Fe²⁺ ion at cathode side and one H⁺ ion at anode side in each single LCFC. When this

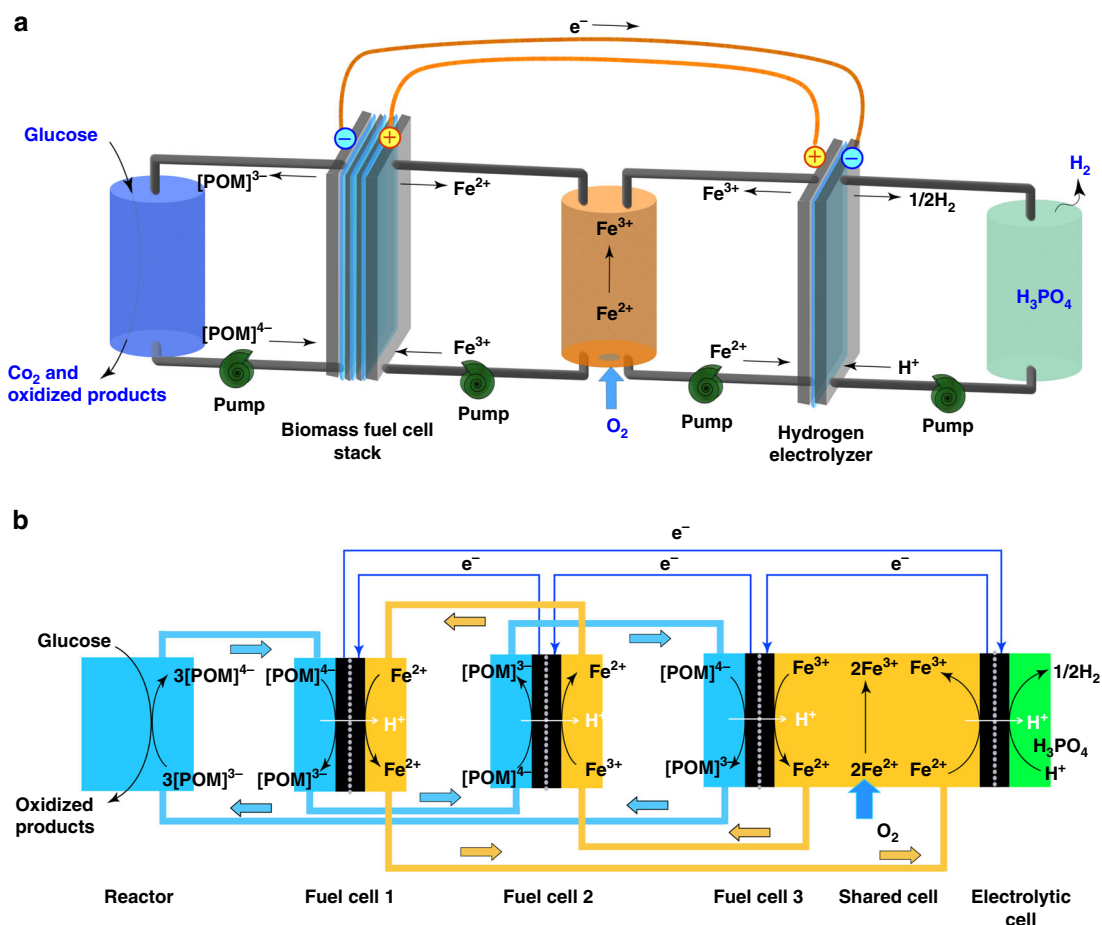
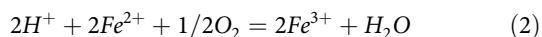


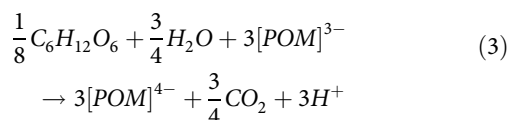
Fig. 1 Conception of the integrated device. **a** Schematic illustration of the integration of REACTORS (stored glucose-POM solution and H₃PO₄ solution in the left and right side respectively), LCFCs (biomass fuel cell stack), PEMEC (hydrogen electrolyzer) and SHAREDCELL (the tank stored Fe²⁺/Fe³⁺ solution in the middle), and **b** the detail electron flow analysis in the device

electron is transferred to PEMEC unit, one H⁺ ion is consumed to 1/2H₂ in PEMEC's cathode. Simultaneously, one Fe²⁺ ion is oxidized to Fe³⁺ in PEMEC's anode. According to Fig. 1b, it is clear that to reduce one H⁺ to 1/2H₂, one electron is transferred, but three H⁺ and three Fe²⁺ ions are produced for a LCFC stack with three individual fuel cells, which means two extra H⁺ ions and Fe²⁺ ions will be produced for producing 1/2H₂. In order to balance the charge and ions for a stable process, O₂ or air is pumped to the SHAREDCELL to react with excess Fe²⁺ and H⁺ ions as the follows:

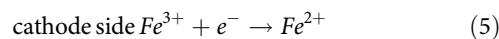


As shown in Fig. 1, by combing four key units of REACTOR, LCFCs, PEMEC and SHAREDCELL together, both polyoxymetallate and iron ions can be completely regenerated, so the concentrations of Fe³⁺/Fe²⁺ and [POM]³⁻/[POM]⁴⁻ are kept in steady state during the process in the integrated device. For an ideal case in which the glucose is completely consumed and the reactions involved in the entire system (three fuel cell stack) are

REACTOR :

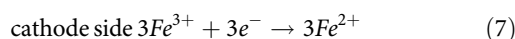
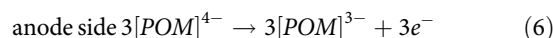


LCFC: For each individual fuel cell (fuel cell-1, 2, and 3):

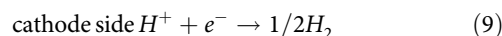
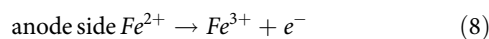


Therefore, for a stack of three fuel cells in a series, the reaction will be

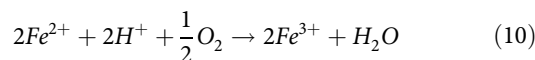
LCFC STACK:



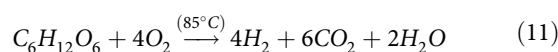
PEMEC:



SHAREDCELL:



THE NET REACTION: (the sum of Eqs. (3), (6)–(10))



It should be noted that at ideal condition, the H₃PO₄ in the cathode cell only serves as buffer which will not be consumed, and all H⁺ are actually from the oxidation reactions of biomass and water in the anodes of the fuel cell stack, as shown in Eq. (3).

It should be noted that our integrated device is different from any previous reported. It is not a simple physical connection of an independent fuel cell with an independent electrolyzer using electric wires. Instead, the fuel cell and electrolyzer are dependant one to another by using a SHAREDCELL. If it is a simple physical connection of an independent fuel cell and an electrolyzer, the electrolytes in both cells have to be regenerated using external electric power or chemical reaction. However, by using a SHAREDCELL, the consumed Fe^{2+} can be self-regenerated as indicated by the Eqs. (3)–(10). As a result, no external electricity is needed in a continuous operation process. This type of integrated process and device has not been reported previously.

To speedup the reactions, the entire solution was heated to 85 °C. It should be noted that because no further cold water will be added to the cells but only solid sugar is continuously fed to the cells, the energy used for heat the solution to 85 °C is only a one-time requirement. If the reaction tank is well insulated, no further heat is needed to maintain the temperature at 85 °C. In other words, there will be no thermal energy consumption during the process if a thermal insulation is used.

Performance and stability of the integrated device. To determine how many fuel cells in a series can provide enough input voltage and current to PEMEC for hydrogen evolution, the fuel cell number and their performance in a LCFC stack was firstly studied. From Fig. 2a, the measured open-circuit voltage in a single cell of LCFC was ca. 0.33 V. When different numbers of single cells in series were assembled into a LCFC stack, the open-circuit voltage increased linearly (black bars in Fig. 2a). However, when the LCFCs unit was connected with a PEMEC unit to form an

integrated device, the LCFCs output voltage (=PEMEC input voltage, red bars in Fig. 2a) was lower than the open circuit voltage.

For the purpose of understanding the PEMEC performance, a separated test of PEMEC unit under different input electric fields (power was provided by an electrochemical workstation rather than LCFCs) was conducted and the I - V curve is shown in Fig. 2b. It can be found that the onset applied voltage in PEMEC was 0.72 V, suggesting that hydrogen could start to form at a supplied voltage greater than 0.72 V. It should be noted that although the standard water split voltage is 1.23 V, the actual reaction of this PEMEC is not pure water split but the combination of reaction (6) and (7) so the electrolysis voltage of this PEMEC is much lower than pure water split. Comparing with the results of Fig. 2a, we concluded that at least four single LCFCs should be connected in series to maintain an output voltage higher than 0.72 V (the critical voltage for electrolysis of PEMEC).

The output currents of LCFCs stack are affected by the total electrode area and running temperature. As shown in Fig. 2c, while increasing the total electrode area of LCFCs from 4 to 12 cm^2 , the output currents of cell stack increased a lot at running temperature of both 20 and 85 °C. But further increasing total electrode area to 36 cm^2 , the output current was improved little. From Fig. 2d, the output current of LCFCs with total electrode area of 12 cm^2 increased significantly while the cell running temperatures were increased. The similar results were observed for LCFCs with 4 and 36 cm^2 electrode areas, as shown in Supplementary Fig. 2. Because the increase of cell running temperature results in an increase of internal energy of electrolytes and a decline of activation polarization²⁷, higher running

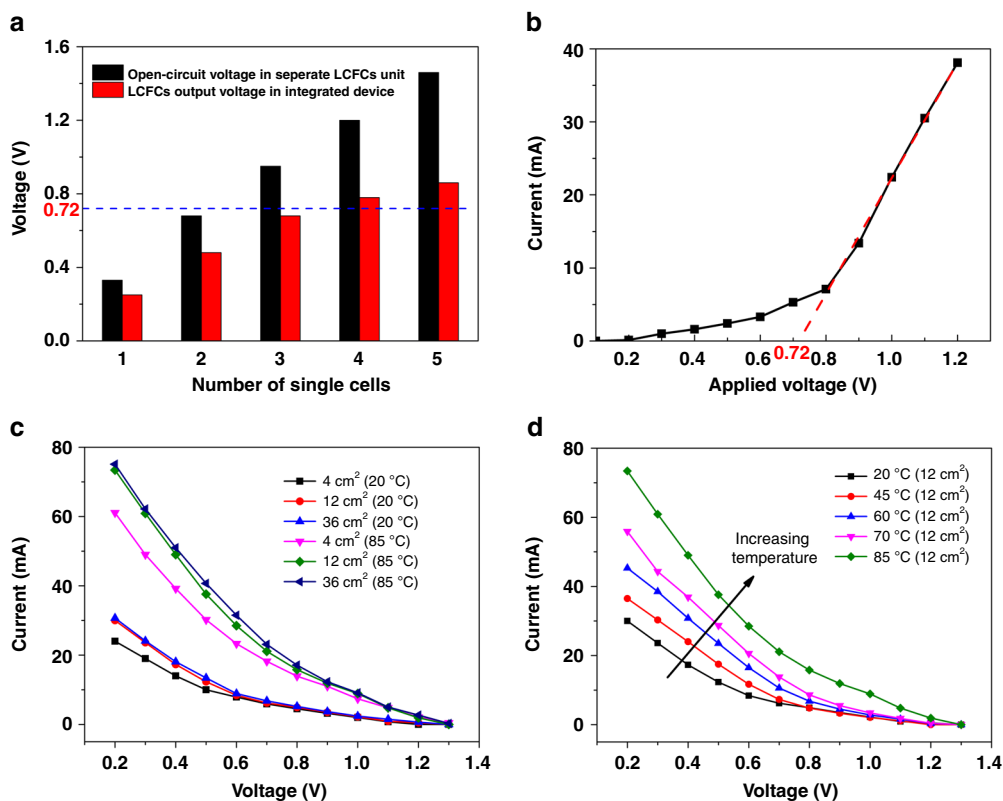


Fig. 2 Design of LCFCs stack. **a** Effect of single cell numbers of LCFCs on open-circuit voltage in separate LCFCs unit and LCFCs output voltage (=PEMEC input voltage) in the integrated device at 20 °C, respectively; the blue broken line marks the onset applied voltage value of 0.72 V in PEMEC. **b** Polarization curve in separate PEMEC unit at 20 °C; the black line is the experimental I - V curve in a PEMEC, and the red broken line is to determine the onset applied voltage in PEMEC. **c** Voltage-current plots in separate LCFCs unit with different total electrode area at 20 and 85 °C, respectively; **d** Voltage-current plots in separate LCFCs unit with electrode area of 12 cm^2 at different running temperatures

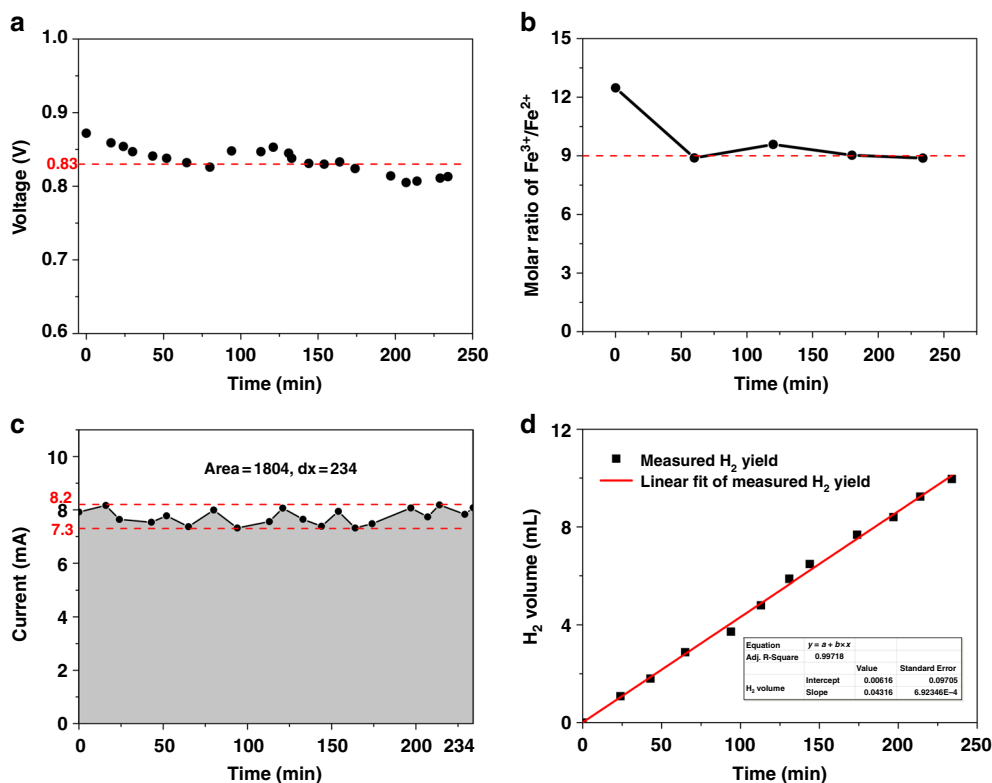


Fig. 3 Stability test of the integrated device. **a** measured LCFCs output voltage (equals to PEMEC input voltage) vs. time; the black points are experimental output voltages of LCFCs, and the red broken line marks the output voltages fluctuating around the value of 0.83 V. **b** molar ratio of Fe³⁺/Fe²⁺ vs. time; the red broken line marks the Fe³⁺/Fe²⁺ ratios keeping stable around a value of 9. **c** measured current in the closed electric circuit vs. time; the red broken lines mark the currents fluctuating within a narrow range of 7.3–8.2 V. And **d** measured H₂ yield vs. time

temperature in LCFCs leads to lower ionic resistance and higher redox rate, so an increase in the output currents of cell stack.

A PEMEC with 1 cm³ cell volume and a LCFCs stack with 4 single cells and 12 cm² total electrode area were combined together and constructed into an integrated device, which was used to perform the continuous test running at 85 °C for 4 h, as shown in Fig. 3. In Fig. 3a, measured LCFCs output voltages slightly fluctuated around the value of 0.83 V during the test, indicating the output voltage of LCFCs in the integrated device could keep stable. In other words, the PEMEC unit can be afforded stable input voltage from LCFCs to maintain hydrogen evolution within 4 hour testing time. To fully test the device performance and the stability, long time tests should be done in future.

The absorbance of Fe-phenanthroline complex at the wavelength of 510 nm can be utilized to determine Fe²⁺ concentration because of the linear relationship between the absorbances at 510 nm and Fe²⁺ concentrations, as shown in Supplementary Fig. 3a. The measured Fe²⁺ concentrations in the Fe³⁺-Fe²⁺ solution tank during test are shown in Supplementary Fig. 3b. From measured Fe²⁺ concentrations, the corresponding molar ratios of Fe³⁺/Fe²⁺ could be calculated, which are shown in Fig. 3b. The measured Fe³⁺/Fe²⁺ ratios dropped quickly at the beginning of the test, then kept stable around a value of 9. It should be noted that the ratio of Fe³⁺/Fe²⁺ in the SHAREDCELL unit is critically important. According to Nernst Equation,

$$\phi = \phi^{\circ} + \frac{RT}{F} \ln \frac{[Fe^{3+}]}{[Fe^{2+}]} \quad (12)$$

if the ratio of Fe³⁺/Fe²⁺ is too high, the electrochemical potential of Fe³⁺-Fe²⁺ solution in SHAREDCELL unit would be also high. As a result, higher voltage for electrolysis in PEMEC is

required for hydrogen formation. In other words, the reaction rate of Fe²⁺+H⁺=Fe³⁺+1/2H₂ in PEMEC unit will be slowed down, and eventually, Fe²⁺ will not be regenerated to Fe³⁺, and the hydrogen production will be stopped. On the other hand, if the ratio of Fe³⁺/Fe²⁺ is too low, the Fe³⁺-Fe²⁺ solution potential in SHAREDCELL unit would be low too. Thus, because the output voltage of LCFCs equals to the difference between electrochemical potential of Fe³⁺/Fe²⁺ and [POM]³⁻/[POM]⁴⁻ pairs, the LCFCs stack will not provide high enough output voltage (>0.72 V in this study) for hydrogen production. Therefore, the steady ratio of Fe³⁺/Fe²⁺ redox pair in SHAREDCELL unit is very important to maintain the stable hydrogen yield by the whole integrated device system. The recycling of Fe³⁺ is partially contributed by the self-regeneration in anode of electrolytic cell and at the same time by the oxidation reaction with oxygen in air. Although the oxidation rate of Fe²⁺ by O₂ is relatively slow in acid solutions, it can be speeded up by using co-catalyst such as Cu-SO₂ which has been reported in previous research²⁸. Our calculation indicates that with the co-catalyst, the regeneration rate of Fe³⁺ could be faster than Fe²⁺ consuming rate in the SHAREDCELL (see Fig. 1). In this study, because the total reaction time is a few hours and no obvious Fe²⁺ concentration change was noticed, so the co-catalyst Cu-SO₂ was not used.

As shown in Fig. 3c, the current (equals to LCFCs output current or PEMEC input current) of the integrated device could almost keep stable during the test with a small fluctuation within a narrow range of 7.3–8.2 mA. This result not only confirms the stable regeneration circle of Fe³⁺/Fe²⁺ in SHAREDCELL unit, but also proves the stable equilibrium between releasing electrons at LCFCs anode and capturing electrons at PEMEC cathode.

The producing H_2 gas was collected and measured by water displacement method. In Fig. 3d, it can be found that the H_2 production rate remained stable during the test, indicating the transferring proton rate could keep a steady dynamic equilibrium with the receiving electron rate to continuously form H_2 gas at PEMEC cathode. Moreover, it can be further inferred that the reaction rate of glucose to release protons and electrons in REACTOR is fast enough to provide a stable hydrogen production rate at PEMEC cathode during the stability test.

Furthermore, as shown in Fig. 3d, a steady pure hydrogen production rate of $0.0432 \text{ mL min}^{-1}$ based on 1 cm^3 cell volume of PEMEC (about $62.2 \text{ m}^3 \text{ H}_2/\text{m}^3/\text{d}$ based on PEMEC volume) can be obtained in our integrated device, which is almost 26 times higher than that of MEC-based system using glucose reported in literature²². The higher hydrogen production rate in our integrated device could be attributed to using POM catalyst to substitute for exoelectrogenic microbes, because POM catalysts have higher reaction activity with glucose than microbe catalysts²⁴.

The total electrons transferred from LCFCs to PEMEC via external circuit can be obtained from the current-time integral area in Fig. 3c. After 234 minutes running time, 108.2 coulomb electrons were transferred in the integrated device. In case of the ideal condition that all the transferred electrons are captured by protons to produce hydrogen gas, the theoretical yield of H_2 could be calculated as 0.561 mmol ($=12.56 \text{ mL}$) during the test according to Faraday-Matteucci's laws:

$$n = \left(\frac{Q}{F}\right) \left(\frac{1}{2}\right) \quad (Q \text{ is total electric charge, and } F \text{ is the Faraday constant}) \quad (13)$$

Experimentally, the measured H_2 yield was 9.96 mL during the test, as shown in Fig. 3d. Therefore, the Faraday efficiency, defined as the ratio of measured to theoretical yield of H_2 , was 79.3% , which means that 79.3% of the electric current generated from the feedstock glucose is used to produce hydrogen by PEMEC in the integrated device.

Glucose functions as fuels that provides energy to drive LCFC and hydrogen donor for hydrogen production in PEMEC. However, glucose was not directly oxidized on graphite anode electrode because of lack of catalyst for glucose oxidation. POM reacted with glucose and worked as charge carrier that transfers electrons from glucose to electrode (verified by cyclic voltammogram (CV) of POM-glucose solution, as shown in Supplementary Fig. 5). In order to investigate final products of glucose decomposition with PMo_{12} after continuous running, the glucose- PMo_{12} solution was continuously heated under reflux in 85°C water bath for over 10 h under N_2 atmosphere. The liquid samples before and after reaction were characterized by $^1\text{H-NMR}$. It is known that the native D-glucose has only two anomers, generally cited as 36% for the $\alpha\text{-D-glucose}$ and 64% for the $\beta\text{-D-glucose}$ ²⁹. From the $^1\text{H-NMR}$ spectra (shown in Fig. 4 a, b), it can be observed that after the long-time reaction with PMo_{12} at 85°C , the specific peaks assigned to $\alpha\text{-}$ and $\beta\text{-D-glucose}$ completely disappeared and the peaks assigned to alcoholic hydroxyl group at $3.1 \sim 3.9 \text{ ppm}$ were also almost disappeared, but only a new peak arose at 7.8 ppm assigned to aldehyde group^{24,29}. The result indicates the two glucose anomers firstly changed into open-chain structure and then were oxidized to low molecular derivatives with aldehyde groups, as shown in Supplementary Fig. 4. Previous researches also confirmed that the major products of biomass (e.g. starch, glucose and cellulose) reacted with POM catalysts in aqueous solution were aldehydes and organic acids^{23,24,26}. In addition, the emission gas from the reaction was collected using a sampling gas bag and analyzed by

gas chromatography (GC). As shown in Fig. 4c, carbon dioxide was the only emission gas product and its percentage was 1.3% that is significantly higher than the value in dry air (0.04%), indicating that glucose was oxidized to CO_2 by PMo_{12} . Because glucose was used as the only feeding raw material, the total organic carbon (TOC) analysis showed that 88% weight of the initial 5.4 g of glucose was degraded to CO_2 after 10 h reaction with 100 mL of 0.3 mol L^{-1} of PMo_{12} at 85°C (shown in Fig. 4d). During the glucose oxidation process, POM maintains the integrated structure (verified by UV-vis spectra shown in Supplementary Fig. 6) because it is a robust and self-healing catalyst, hundreds of thousands of turnovers are possible³⁰⁻³².

The adopted PMo_{12} catalyst is tolerant to catalyst-poisoning contaminations because POMs are robust and self-healing³³⁻³⁵. Borrás-Almenar et al. also indicated that for the reaction mixture containing the substrate and the POM catalyst, hundreds of thousands of turnovers are possible³². So the PMo_{12} catalyst can be continuously regenerated and used in this integrated device. As a result, if the reaction is continuous long enough, it is believed that glucose will be completely degraded to CO_2 eventually.

Discussion

In summary, we demonstrated the feasibility of fabricating an integrated electrolysis device that can effectively convert glucose to pure hydrogen without any external electric power supply at a low temperature of 85°C . The electric energy applied to the electrolyzer is directly from a glucose-based flow fuel cell. Our integrated device is not a simple connection of an electrolyzer and a flow fuel cell through an external electric circuit. Instead, the presented design introduced a SHAREDCELL which functions as not only the cathode of the flow fuel cell but also the anode of electrolyzer. The net reaction of the process is completely converting glucose to hydrogen and CO_2 gases through oxygen oxidation at low temperature ($\sim 85^\circ\text{C}$), which cannot be achieved by a simply combination of a flow cell with an electrolyzer. This is due to the factor that glucose cannot be directly used as fuel in a traditional fuel cell because it cannot be completely converted to CO_2 even in the presence of noble-metal catalyst. With this design, part of the cathode electrolyte (Fe^{3+}) in the flow fuel cell and anode electrolyte (Fe^{2+}) in the electrolyzer are self-regenerated without external power supply. To the best of our knowledge, no any similar design has been reported in literature. It has been known that PEMEC can produce high purity hydrogen gas ($>99.99 \text{ vol.}\%$) without any auxiliary purification equipment^{36,37}. Our integrated device also produced pure H_2 without any detectable impurity based on the results of GC analysis (Supplementary Fig. 7). Besides, the anodes of our integrated electrolyzer are free of noble-metal catalyst (Supplementary Table 1). Although only glucose was tested in this study, based on our previous study^{23,24,26}, we believe that many raw biomasses, such as starch, cellulose, grass and wood powders can also be used in this device without extra chemical pre-treatment and purification, which would significantly reduce the feedstock cost.

Methods

Preparation of electrolyte solution. Phosphomolybdic acid ($\text{H}_3[\text{PMo}_{12}\text{O}_{40}]$, noted as PMo_{12}) with $\alpha\text{-Keggin}$ structure was purchased from TCI America. D-Glucose powder and $\text{FeCl}_3 \cdot 6\text{H}_2\text{O}$ were purchased from AMRESCO America. The glucose- PMo_{12} solution was synthesized by mixing 2 mol L^{-1} glucose and 0.3 mol L^{-1} PMo_{12} solution with magnetic stirring until dissolved. The glucose- PMo_{12} solution was pretreated under reflux in 85°C water bath for 5 h, then the color of the solution turned from yellow to deep blue. The Fe^{3+} - Fe^{2+} solution was obtained by adding 10.8 g $\text{FeCl}_3 \cdot 6\text{H}_2\text{O}$ to 4 mL 37% hydrochloric acid and then diluting to 40 mL . The total concentration of Fe^{3+} and Fe^{2+} was 1 mol L^{-1} .

Assembly of separate LCFCs and test methods. The bipolar plates of LCFCs were made of the high-density graphite plates with specific flow channels. There

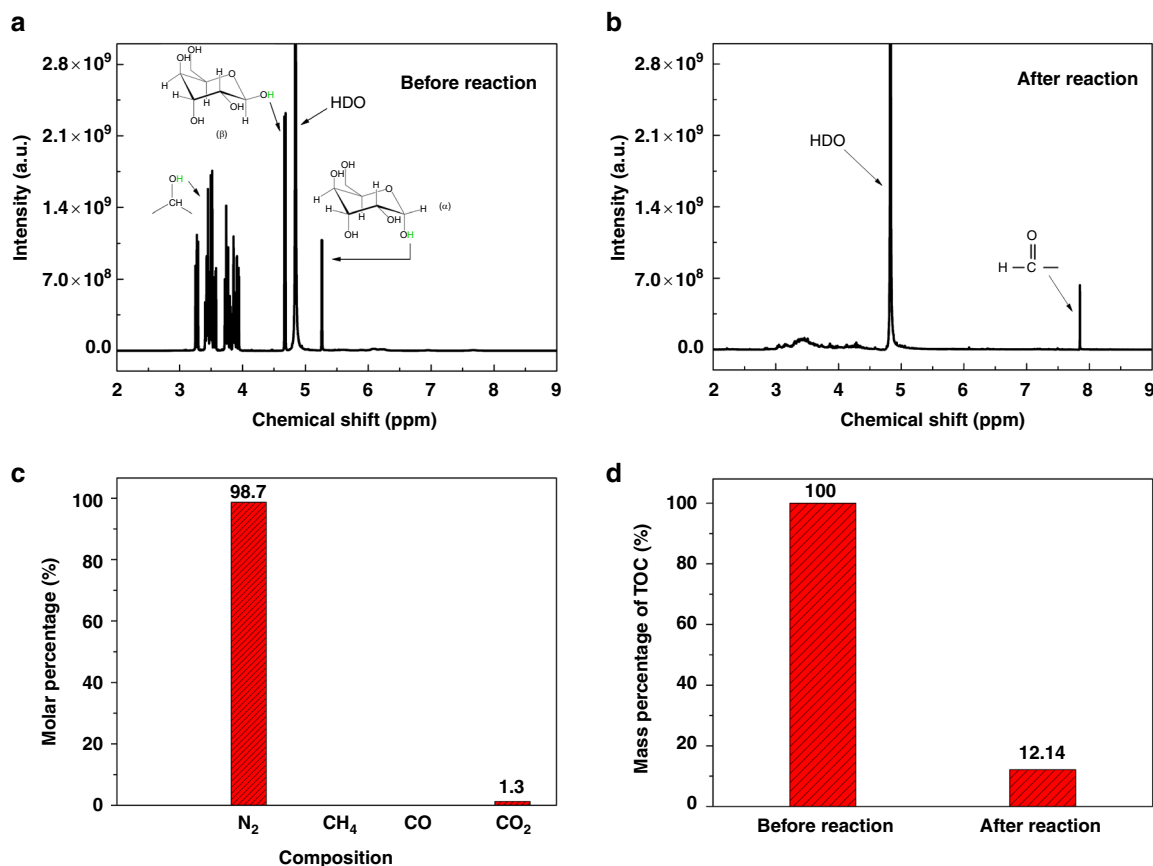


Fig. 4 Glucose degradation with PMo_{12} for long time reaction. **a, b** ^1H NMR spectra of liquid samples before and after reaction (solvent D_2O); **c** composition analysis of emission gas by GC; **d** TOC percentage of liquid samples before and after reaction

are three types of flow channels on the graphite plates. The first is a serpentine flow channel of 5 cm long, 2 mm wide and 10 mm deep (total geometrical projected flow-field area of 1 cm^2); the second is a square flow channel of 3 cm wide, 3 cm long and 10 mm deep (total geometrical projected flow-field area of 9 cm^2) and the third is a square flow channel of 5 cm wide, 5 cm long and 5 mm deep (total geometrical projected flow-field area of 25 cm^2). All bipolar plates were not coated with any catalyst in the flow channels. Nafion 115 (127 μm thick, purchased from FuelCellsEtc) was used as proton exchange membrane in the fuel cell. The membrane was pretreated in the boiling solution of $1\text{ mol L}^{-1}\text{ H}_2\text{SO}_4$ and $3\% \text{ H}_2\text{O}_2$ for 30 min, then washed and soaked in DI water. For every single fuel cell, the Nafion membrane was sandwiched between two graphite plates, which were clamped between two aluminum end plates.

The PVC fittings were used as insulators to avoid the direct contact of graphite plates with end plates. Meanwhile, the PVC gaskets were included on the circumference of the graphite flow-field plates to prevent any leakage. The PVC tubes were used to connect the graphite plate with the external tank through a pump that can transport electrolyte solutions into and out of the flow channel on graphite plates. Details of fabricating single LCFC were reported in our previous studies²³.

To assemble LCFCs, the different number of single cells with different flow-field areas were combined together in series. For example, the LCFCs with four single cells and total flow-field area of 12 cm^2 could be assembled by choosing three single cells with flow-field area of 1 cm^2 and one single cell with 9 cm^2 to be combined in series. The glucose- PMo_{12} solution and Fe^{3+} - Fe^{2+} solution were stored in the anode and cathode tank respectively. The anode electrolyte was pumped to flow through every anode graphite plate of single cells in turn and then back to the anode tank. So did cathode electrolyte. The electrolyte tanks used glass vessels. The temperatures of the electrolytes were controlled to range from 20 to 85°C by heating the electrolyte tanks. The flow rates of the anode and cathode electrolyte were all 20 mL min^{-1} .

While varying the single cell numbers, total flow-field areas and running temperatures of separate LCFCs, the open-circuit voltages were measured using a standard multimeter (DT9602R Auto/Manual Digital Multimeter, TekPower), and the I - V curves were obtained on the CHI 660E Electrochemical Workstation (CH Instruments) using the controlled multi-potential steps method.

Assembly of separate PEMEC and test methods. The electrode plates of the PEMEC were made of high-density graphite plates with a square flow channel of

1 cm long, 1 cm wide and 10 mm deep (electrolysis cell volume of 1 cm^3). The anode plate was not coated any catalyst in the flow channel. But the cathode plate was coated with Pt black catalyst in the flow channel by two-steps reduction method: firstly the Cu metal film was formed in the flow channel of graphite plate by electroplating CuSO_4 solution, then the Cu film was substituted with Pt coating by in-situ chemical reduction of H_2PtCl_6 solution.

To assemble the PEMEC, the Nafion 115 membrane was sandwiched between the anode plate without coating any catalyst and the cathode plate coated with Pt black catalyst for H_2 evolution. The electrode plates were clamped between two aluminum end plates and PVC fittings were used to avoid the direct contact of graphite plates and end plates. PVC gasket was also used on the circumference of the graphite flow-field plates to avoid any leakage. The $1\text{ mol L}^{-1}\text{ Fe}^{3+}$ - Fe^{2+} solution and $1\text{ mol L}^{-1}\text{ H}_3\text{PO}_4$ solution were used as electrolytes and stored in anode and cathode tank respectively. For the separate PEMEC, a CHI 660E Electrochemical Workstation (CH Instruments) was used to provide power to examine the I - V curves using the controlled multi-potential steps method.

Assembly of the integrated device and test methods. To assemble an integrated device, combining the separate LCFCs and the separate PEMEC together by using the same Fe^{3+} - Fe^{2+} solution tank to afford electrolyte to pump through LCFCs cathode electrode and PEMEC anode electrode in turn, then back to the tank. And the glucose- PMo_{12} solution and $1\text{ mol L}^{-1}\text{ H}_3\text{PO}_4$ solution were still pumped through LCFCs anode electrode and PEMEC cathode electrode respectively. Meanwhile, the LCFCs anode to PEMEC cathode and LCFCs cathode to PEMEC anode were connected by electrical wires to form a closed electric circuit. The physical pictures and layout details are shown in Supplementary Fig. 1. The volume ratio of glucose- PMo_{12} , Fe^{3+} - Fe^{2+} and H_3PO_4 electrolyte was 100:3-5:10, and the flow rates of electrolytes were all 20 mL min^{-1} .

While varying the single cell numbers of LCFCs in the integrated device, the LCFCs output voltages (=PEMEC input voltages) were measured using a DT9602R Auto/Manual Digital Multimeter (TekPower US). All the data were collected after the integrated device running for 15 min.

Stability test for the integrated device and test methods. A PEMEC with 1 cm^3 cell volume and a LCFCs stack with 4 single cells and 12 cm^2 total electrode area were combined together and constructed into an integrated device, which was used to perform the continuous test running at 85°C for 4 h. 1000 mL glucose- PMo_{12} ,

40 mL Fe^{3+} - Fe^{2+} and 100 mL H_3PO_4 solution were used as three electrolytes to afford the device running. The glucose- PMO_{12} solution was always controlled at 85 °C in the stability test, indicating the excessive glucose could continue to react with the oxidized state of PMO_{12} during test. The Fe^{3+} - Fe^{2+} tank was also controlled at 85 °C and open to contact with O_2 gas. The outlet hydrogen gas at PEMEC cathode side was collected by water displacement, and the rate of hydrogen production was followed by gas-volume measurements²⁶.

During stability test, the LCFs output voltages were measured using a DT9602R Auto/Manual Digital Multimeter (TekPower US) in parallel mode. The currents in the closed electric circuit were measured in series mode using another DT9602R Auto/Manual Digital Multimeter. To determine the molar ratio of $\text{Fe}^{3+}/\text{Fe}^{2+}$ during the test, the Fe^{2+} concentrations of samples obtained from Fe^{3+} - Fe^{2+} tank were measured by UV-visible spectrophotometry. A 0.50 mL sample was firstly diluted to 50 mL in a volumetric flask. Then pipet 1.00 mL diluted sample solution, 5.00 mL HAc-NaAc buffer solution (pH = 5.0) and 2.00 mL 0.15% 1,10-phenanthroline solution into a 50 mL colorimetric cylinder and dilute to the mark with DI water. After placing for 10 min, the absorbance at 510 nm was measured by using the Agilent 8453 UV-visible spectrophotometer. A series of standard Fe^{2+} solutions, ranging from 0 to 27 $\mu\text{mol L}^{-1}$, were also carried through the procedure and used to calibrate the method. Because the total concentration of Fe^{3+} and Fe^{2+} was 1 mol L^{-1} , the molar ratio of $\text{Fe}^{3+}/\text{Fe}^{2+}$ could be calculated.

Glucose degradation with PMO_{12} for long-time reaction and product characterizations.

In total 0.03 mol glucose powder was added to 100 mL 0.3 mol L^{-1} PMO_{12} solution with magnetic stirring until dissolved. Then the glucose- PMO_{12} solution was transferred to a flask and air in the reactor was purged out by pure N_2 gas. And the reactor was always protected from air under nitrogen atmosphere while the solution was continuously heated under reflux in 85 °C water bath for over 10 h. The emission gas passed through the reflux condensing tube was collected using a sampling gas bag. The composition of gas product was analyzed on Agilent 490 Micro GC with a four-channel system, helium carrier gas and TCD detector.

The liquid samples before and after long-time reaction were also gathered. And the samples were dried at 70 °C in vacuum, then re-dissolved in D_2O for ^1H NMR. The ^1H NMR spectra were measured on a Bruker Avance/DMX 400 MHz NMR spectrometer with 16 scans and 1 s pulse delay.

Total organic carbon (TOC) analysis of liquid samples before and after long-time reaction was taken on TOC analyzer (model TOC-L CPN, Shimadzu Corporation).

Data availability

The authors declare that all data supporting the findings of this study are available within in the article and Supplementary Information files, and are also available from the corresponding author upon reasonable request.

Received: 28 October 2018 Accepted: 23 May 2019

Published online: 14 June 2019

References

- Guandalini, G., Campanari, S. & Valenti, G. Comparative assessment and safety issues in state-of-the-art hydrogen production technologies. *Int J. Hydrog. Energy* **41**, 18901–18920 (2016).
- Amirante, R., Cassone, E., Distaso, E. & Tamburrano, P. Overview on recent developments in energy storage: Mechanical, electrochemical and hydrogen technologies. *Energy Conv. Manag* **132**, 372–387 (2017).
- Hosseini, S. E. & Wahid, M. A. Hydrogen production from renewable and sustainable energy resources: Promising green energy carrier for clean development. *Renew. Sust. Energ. Rev.* **57**, 850–866 (2016).
- Nikolaïdis, P. & Poullikkas, A. A comparative overview of hydrogen production processes. *Renew. Sust. Energ. Rev.* **67**, 597–611 (2017).
- de Wit, M. & Faaij, A. European biomass resource potential and costs. *Biomass- Bioenergy* **34**, 188–202 (2010).
- Williams, A., Jones, J. M., Ma, L. & Pourkashanian, M. Pollutants from the combustion of solid biomass fuels. *Prog. Energy Combust. Sci.* **38**, 113–137 (2012).
- Kan, T., Strezov, V. & Evans, T. J. Lignocellulosic biomass pyrolysis: A review of product properties and effects of pyrolysis parameters. *Renew. Sust. Energ. Rev.* **57**, 1126–1140 (2016).
- Parthasarathy, P. & Narayanan, K. S. Hydrogen production from steam gasification of biomass: Influence of process parameters on hydrogen yield – a review. *Renew. Energy* **66**, 570–579 (2014).
- Wang, S. R., Dai, G. X., Yang, H. P. & Luo, Z. Y. Lignocellulosic biomass pyrolysis mechanism: a state-of-the-art review. *Prog. Energy Combust. Sci.* **62**, 33–86 (2017).

- Liu, C. J., Wang, H. M., Karim, A. M., Sun, J. M. & Wang, Y. Catalytic fast pyrolysis of lignocellulosic biomass. *Chem. Soc. Rev.* **43**, 7594–7623 (2014).
- Demirbas, M. F. Technological options for producing hydrogen from renewable resources. *Energy Sources, Part A: Recovery, Util., Environ. Eff.* **28**, 1215–1223 (2006).
- Ren, N. Q., Zhao, L., Chen, C., Guo, W. Q. & Cao, G. L. A review on bioconversion of lignocellulosic biomass to H₂: key challenges and new insights. *Bioresour. Technol.* **215**, 92–99 (2016).
- Urbaniec, K. & Bakker, R. R. Biomass residues as raw material for dark hydrogen fermentation-A review. *Int J. Hydrog. Energy* **40**, 3648–3658 (2015).
- Singh, A. et al. Biohydrogen production from lignocellulosic biomass: technology and sustainability. *Energies* **8**, 13062–13080 (2015).
- Puga, A. V. Photocatalytic production of hydrogen from biomass-derived feedstocks. *Coord. Chem. Rev.* **315**, 1–66 (2016).
- Ghimire, A. et al. A review on dark fermentative biohydrogen production from organic biomass: Process parameters and use of by-products. *Appl. Energy* **144**, 73–95 (2015).
- Kadier, A., Simayi, Y., Kalil, M. S., Abdeshahian, P. & Hamid, A. A. A review of the substrates used in microbial electrolysis cells (MECs) for producing sustainable and clean hydrogen gas. *Renew. Energy* **71**, 466–472 (2014).
- Selemba, P. A., Perez, J. M., Lloyd, W. A. & Logan, B. E. High hydrogen production from glycerol or glucose by electrohydrogenesis using microbial electrolysis cells. *Int J. Hydrog. Energy* **34**, 5373–5381 (2009).
- Kadier, A. et al. A comprehensive review of microbial electrolysis cells (MEC) reactor designs and configurations for sustainable hydrogen gas production. *Alex. Eng. J.* **55**, 427–443 (2016).
- Lu, L., Xing, D. F., Ren, N. Q. & Logan, B. E. Syntrophic interactions drive the hydrogen production from glucose at low temperature in microbial electrolysis cells. *Bioresour. Technol.* **124**, 68–76 (2012).
- Kadier, A. et al. Recent advances and emerging challenges in microbial electrolysis cells (MECs) for microbial production of hydrogen and value-added chemicals. *Renew. Sust. Energ. Rev.* **61**, 501–525 (2016).
- Zhang, J. N., Bai, Y. X., Fan, Y. T. & Hou, H. W. Improved bio-hydrogen production from glucose by adding a specific methane inhibitor to microbial electrolysis cells with a double anode arrangement. *J. Biosci. Bioeng.* **122**, 488–493 (2016).
- Liu, W., Mu, W. & Deng, Y. High-performance liquid-catalyst fuel cell for direct biomass-into-electricity conversion. *Angew. Chem.* **53**, 13558–13562 (2014).
- Liu, W. et al. Solar-induced direct biomass-to-electricity hybrid fuel cell using polyoxometalates as photocatalyst and charge carrier. *Nat. Commun.* **5**, 3208 (2014).
- Gong, J. et al. Direct Conversion of Wheat Straw into Electricity with a Biomass Flow Fuel Cell Mediated by Two Redox Ion Pairs. *ChemSuschem* **10**, 506–513 (2017).
- Liu, W. et al. High efficiency hydrogen evolution from native biomass electrolysis. *Energy Environ. Sci.* **9**, 467–472 (2016).
- Jang, J. H., Chiu, H. C., Yan, W. M. & Sun, W. L. Effects of operating conditions on the performances of individual cell and stack of PEM fuel cell. *J. Power Sources* **180**, 476–483 (2008).
- Zhang, W., Muir, D. M. & Singh, P. Iron(II) oxidation by SO_2/O_2 in acidic media: Part II. Effect of copper. *Hydrometallurgy* **58**, 117–125 (2000).
- Gurst, J. E. NMR and the structure of D-glucose. *J. Chem. Educ.* **68**, 1003–1004 (1991).
- Hill, C. L. & Zhang, X. A ‘smart’ catalyst that self-assembles under turnover conditions. *Nature* **373**, 324–326 (1995).
- Pratt, H. D., Hudak, N. S., Fang, X. & Anderson, T. M. A polyoxometalate flow battery. *J. Power Sources* **236**, 259–264 (2013).
- Borrás-Almenar, J. J., Coronado, E., Pope, M. *Polyoxometalate molecular science*. (Springer Science & Business Media, 2003).
- Wang, S. S. & Yang, G. Y. Recent advances in polyoxometalate-catalyzed reactions. *Chem. Rev.* **115**, 4893–4962 (2015).
- Miras, H. N., Vila-Nadal, L. & Cronin, L. Polyoxometalate based open-frameworks (POM-OFs). *Chem. Soc. Rev.* **43**, 5679–5699 (2014).
- Blasco-Ahicart, M., Soriano-Lopez, J., Carbo, J. J., Poblet, J. M. & Galan-Mascaros, J. R. Polyoxometalate electrocatalysts based on earth-abundant metals for efficient water oxidation in acidic media. *Nat. Chem.* **10**, 24–30 (2018).
- Rahim, A. H. A., Tijani, A. S., Kamarudin, S. K. & Hanapi, S. An overview of polymer electrolyte membrane electrolyzer for hydrogen production: Modeling and mass transport. *J. Power Sources* **309**, 56–65 (2016).
- Wang, G. J. et al. Progress on design and development of polymer electrolyte membrane fuel cell systems for vehicle applications: a review. *Fuel Process Technol.* **179**, 203–228 (2018).

Acknowledgements

We thank National Natural Science Foundation of China (51678160, 21576054), Guangdong Province Science and Technology Project (2016A020221033), Guangzhou

Science and Technology Project (201704020202), and Research Fund for Applied Science and Technology of Guangdong (2016B020241003). Wei Liu, Zhe Zhang and Xu Du thank the scholarships from RBI at Georgia Tech.

Author contributions

Y.L. and W.L. designed the experiments and performed the electrolytic hydrogen evolution experiments. Z.Z., X.D. helped to perform NMR and GC analyses. Y.L., W.L., L.Y. and Y.D. contributed to the manuscript preparation and Y.D. charged the project.

Additional information

Supplementary information accompanies this paper at <https://doi.org/10.1038/s42004-019-0169-5>.

Competing interests: The authors declare no competing interests.

Reprints and permission information is available online at <http://npg.nature.com/reprintsandpermissions/>

Publisher's note: Springer Nature remains neutral with regard to jurisdictional claims in published maps and institutional affiliations.



Open Access This article is licensed under a Creative Commons Attribution 4.0 International License, which permits use, sharing, adaptation, distribution and reproduction in any medium or format, as long as you give appropriate credit to the original author(s) and the source, provide a link to the Creative Commons license, and indicate if changes were made. The images or other third party material in this article are included in the article's Creative Commons license, unless indicated otherwise in a credit line to the material. If material is not included in the article's Creative Commons license and your intended use is not permitted by statutory regulation or exceeds the permitted use, you will need to obtain permission directly from the copyright holder. To view a copy of this license, visit <http://creativecommons.org/licenses/by/4.0/>.

© The Author(s) 2019